Ka-Band Wide-Bandgap Solid-State Power Amplifier: Prototype Combiner Spurious Mode Suppression and Power Constraints

P. Khan[1] and L. Epp[1]

Results of prototype hardware activities related to a 120-W, 32-GHz (Ka-band) solid-state power amplifier (SSPA) architecture study are presented. Spurious mode suppression and the power-handling capability of a prototype 24-way radial combiner and a prototype 2-way septum binary combiner were investigated. Experimental data indicate that a commercial absorptive filter, designed to pass the circular TE_{01} mode, effectively suppressed the higher-order modes generated by a narrowband, flower-petal-type mode transducer. However, the same filter was not effective in suppressing higher-order modes generated by the broadband Marie mode transducer that is used in the prototype waveguide radial combiner. Should greater filtering be required by a particular SSPA application, a broadband mode filter that can suppress specifically those higher-order modes that are generated by the Marie transducer will need to be developed. A back-to-back configuration of the prototype radial combiner was tested with drive power up to approximately 50 W. No anomalous behavior was observed. Power measurements of the septum combiner indicate that up to 10-W radio frequency (RF) can be dissipated in the integrated resistive element before a permanent performance shift is observed. Thus, a given adder (a single-stage, 2-way combiner) can safely combine two 20-W sources, and the adder will not be damaged in the event of a source failure. This result is used to calculate the maximum source power that can be safely combined as a function of the number of sources combined and the number of source failures allowed in a multi-stage combiner. The analysis shows that SSPA power >140 W can be generated by power combining 16 sources producing 10 W each. In this configuration, up to three sources could fail with the guarantee that the combiner would not be damaged. Finally, a modified prototype septum combiner design was verified. The improved design reduced the assembly time from over 2 hours to about 15 minutes per adder.

[1] Communications Ground Systems Section.

This research was carried out at the Jet Propulsion Laboratory, California Institute of Technology, and was sponsored by Glenn Research Center, and the National Aeronautics and Space Administration. Reference herein to any specific commercial product, process, or service by trade name, trademark, manufacturer or otherwise, does not constitute or imply its endorsement by the United States Government or the Jet Propulsion Laboratory, California Institute of Technology.

I. Introduction

A. Wide-Bandgap Solid-State Power Amplifier Architecture Study

Recent advances in wide-bandgap (WBG), gallium nitride (GaN) semiconductor technology may enable the development of efficient solid-state power amplifiers (SSPAs) as an alternative to the traveling-wave tube amplifier (TWTA) for space applications. Key goals of the current effort are to assess the technical feasibility of such an SSPA for operation at 32 GHz (Ka-band), estimate the required WBG device performance, and generate a roadmap to an engineering model of the SSPA.

During the initial phase of this work, we investigated power-combining technologies and SSPA architectures that can enable a 120-W, 40 percent power-added efficiency (PAE) SSPA to be developed for operation over a 31- to 36-GHz band [1–4]. The study proposed three candidate architectures for the target SSPA. The proposed architectures are based on a waveguide radial combiner,[2] a septum binary combiner,[3] and a parallel-plate radial combiner.[4] Subsequently, a prototype 24-way waveguide radial combiner and a prototype 2-way septum combiner were designed and fabricated to validate key performance parameters. Both prototype combiners demonstrated excellent port match and insertion loss characteristics over the required frequency band [4]. The measurements validated important RF parameters that directly affect the efficiency of the SSPA and that help establish WBG device requirements.

This article documents the results of follow-on activities to better understand the operation and performance limitations of the prototype waveguide radial and septum binary combiners.

B. Follow-On Activities

Follow-on activities relating to the waveguide radial combiner included measurements pertaining to spurious mode effects and high-power operation. The radial combiner employs a waveguide mode transducer to generate a circularly symmetric field distribution at the power-combining junction of the circuit. The transducer contains overmoded sections in which spurious modes can be excited and trapped. These trapped modes are believed to generate observed spikes in the transfer characteristics of the combiner. The measured insertion loss of the prototype combiner, including the effect of the spurious modes, potentially can meet target SSPA requirements. However, elimination of the spurious modes can significantly improve the combining efficiency. Moreover, system-level implications of these spurious modes have yet to be determined. Therefore, we investigated an approach to suppress trapped modes. The effectiveness of a commercial mode filter to suppress trapped modes was measured for both a commercial, narrowband, flower-petal mode transducer and the broadband Marie transducer specifically designed for the target application. For the high-power test, a back-to-back configuration of a 24-way radial combiner prototype was tested with drive power up to 50 W.

Follow-on activities relating to the septum binary combiner included high-power tests and design improvements for manufacturability. The septum combiner's thin-film resistive element is critical to achieving the excellent small-signal radio frequency (RF) performance previously demonstrated. The resistive element's ability to dissipate heat, however, is an important point of interest. For the high-power test, a prototype 2-way combiner was driven with an asymmetric, large-signal excitation to measure the maximum power that can be safely dissipated by the resistive element. To improve the mechanical design,

---

[2] L. W. Epp, A. R. Khan, D. J. Hoppe, and D. Kelley, *Wideband 24-Way Radial Power Combiner/Divider Fed by a Marie Transducer*, JPL New Technology Report no. 41511 (internal document), Jet Propulsion Laboratory, Pasadena, California, December 7, 2004.

[3] A. R. Khan, L. W. Epp, D. J. Hoppe, and D. Kelley, *Thin-Film Resistive Septum Waveguide Power Combiner*, JPL New Technology Report no. 40903 (internal document), Jet Propulsion Laboratory, Pasadena, California, November 16, 2004.

[4] A. R. Khan, L. W. Epp, and D. J. Hoppe, *Wideband (31 to 36 GHz) Parallel Plate Power Combiner/Divider with Isolation*, JPL New Technology Report no. 41758 (internal document), Jet Propulsion Laboratory, Pasadena, California, January 31, 2005.

a new method of integrating the resistive element with the waveguide structure was validated. The new design decreases the number of substrates that must be separately assembled and significantly reduces the time required to fabricate the septum combiner.

II. Waveguide Radial Combiner Activities

A. Circular Taper Transitions for the Mode Filter

The effectiveness of a commercial circular waveguide mode filter [5] to suppress spurious modes in the prototype waveguide combiner was measured. The mode filter is designed to propagate the desired TE_{01} circular mode and attenuate higher-order spurious modes. A set of linear tapers was manufactured to allow the filter to be inserted between the mode transducer and the power combiner radial base [Fig. 1(a)].

Since the waveguide diameter of the filter and combiner differ by only 0.33 mm, a short, 2.5-cm taper length is sufficient to achieve excellent match. To verify this, a 10-section, stepped-taper model of the transition was analyzed using a commercial mode-matching analysis tool [Fig. 1(b)]. The theoretical match is >57 dB, and the theoretical insertion loss is essentially 0 dB over the design band of 31 to 36 GHz. The analysis also indicates that the desired TE_{01} mode does not couple effectively to higher-order modes and, thus, the taper is not expected to directly generate additional mode impurity.

B. Flower-Petal Transducer Spurious Mode Suppression

In addition to enabling filter measurements, the taper transitions allowed the prototype radial combiner base to be fed by a commercial mode transducer [6]. The transducer design is a "flower-petal" type, described by Hoag et al. [7]. The flower-petal transducer was measured to operate over the 33.5- to 35.5-GHz band. Although the bandwidth does not meet the target SSPA requirements, tests were carried out nonetheless to gain insight into the operation of the combiner base and the mode filter. It should be noted that the mode filter used in our measurements was designed to work in conjunction with this specific flower-petal transducer design. The transducer and filter were both designed to operate at a 34.5-GHz center frequency.

To verify that the filter effectively suppresses spurious modes, two flower-petal transducers were measured in a back-to-back configuration. Two measurements were taken, one with and one without the mode filter inserted between the transducers (Fig. 2). It is clear that the filter is effective in suppressing the spurious spikes occurring at 34.2 and 35.0 GHz in the response of the flower-petal transducer. It is also evident that a single filter inserted between the transducers adds approximately 0.1 dB of additional insertion loss.

Next, two radial bases, each fed by a flower-petal transducer, were measured in a back-to-back configuration. Two measurements were taken, one with and one without a mode filter inserted between each transducer and its radial base (Fig. 3). A photograph of the setup without filters is shown in Fig. 4. As in the back-to-back transducer case discussed above, the filters are effective in suppressing the spurious spikes in the transfer characteristics of back-to-back radial combiners fed by flower-petal transducers. Over the 33.5- to 35.5-GHz band, the worst-case insertion loss of back-to-back combiners without a filter is measured to be 2.1 dB. With a filter, the worst-case insertion loss is 0.5 dB. The spikes are reduced in magnitude from about 1.75 dB to about 0.2 dB. Based on this measurement, the insertion loss of a single radial combiner is estimated to be 0.25 dB, including the mode transducer and filter.

C. Marie Transducer Spurious Mode Suppression

A set of measurements was performed to determine the effectiveness of a mode filter to suppress spurious mode effects in the radial combiner fed by the Marie transducer. The measurements correspond to those done for the flower-petal transducer, as discussed in Section II.B. The same mode filters and

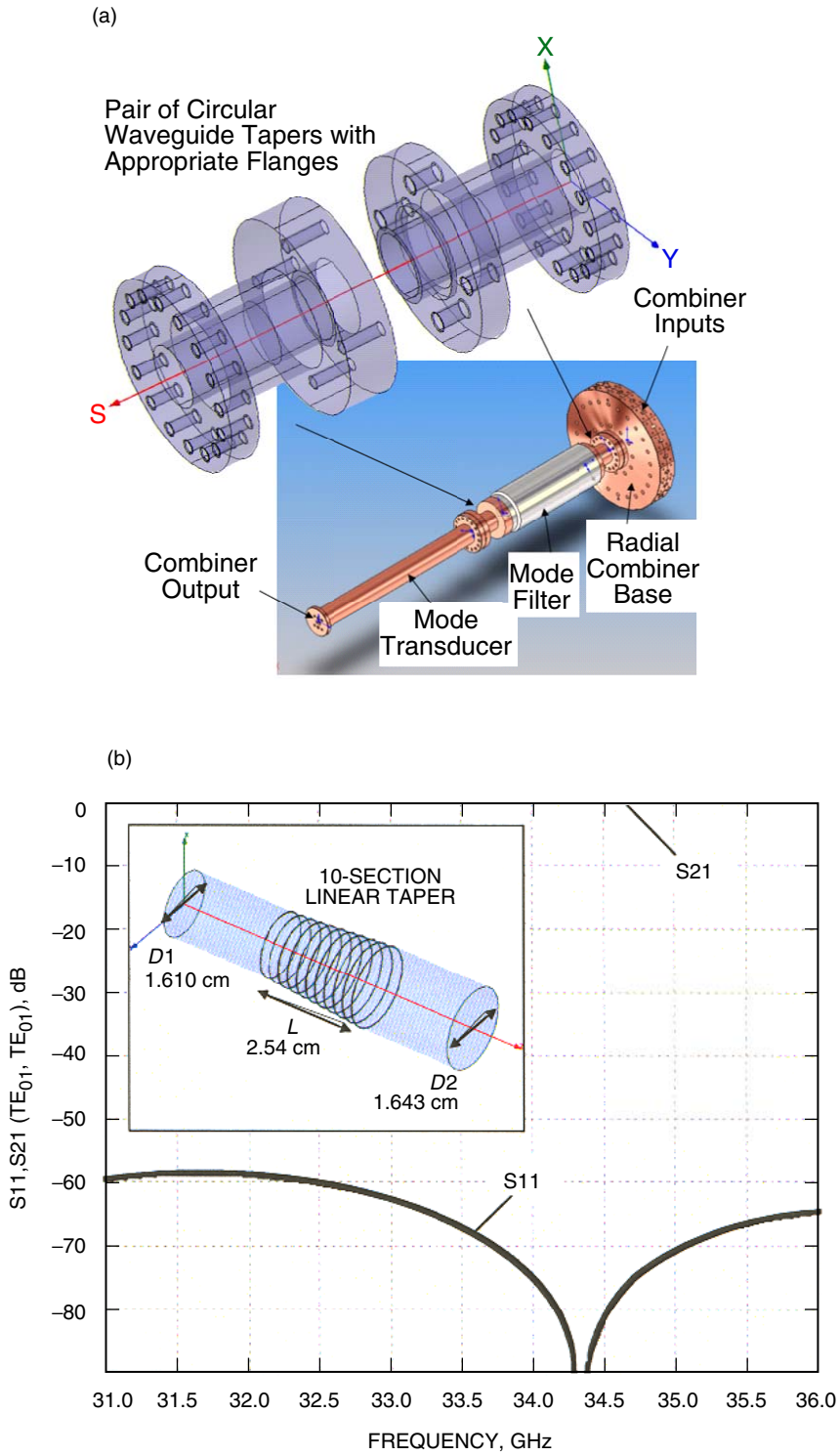

Fig. 1. Geometry showing how the mode filter was adapted to the mode transducer: (a) a pair of taper transitions was used to insert a mode filter between the mode transducer and the combiner base and (b) analysis of a single waveguide taper.

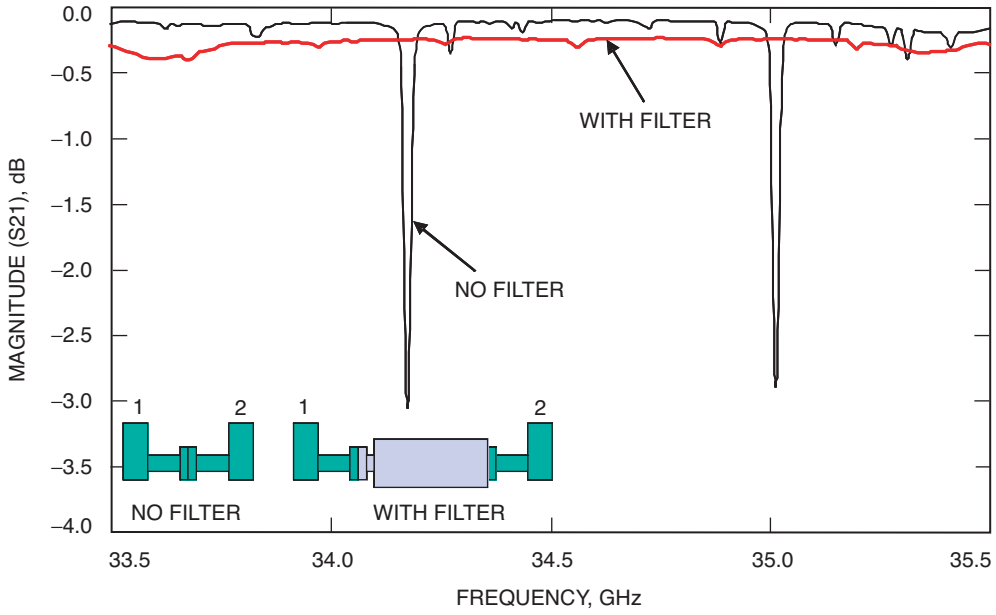

Fig. 2. Back-to-back flower-petal transducers measured with and without a mode filter.

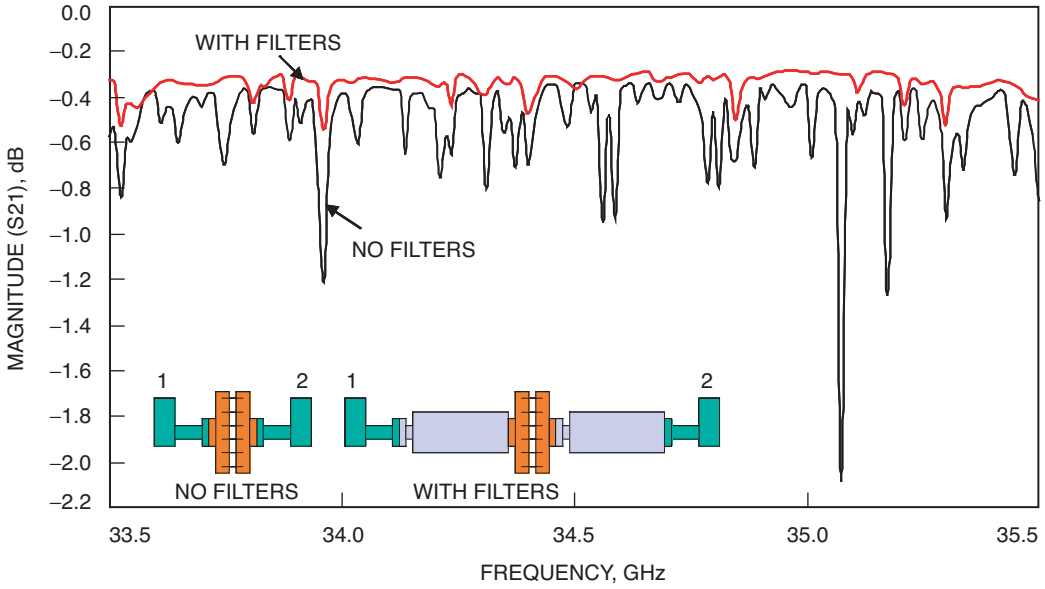

Fig. 3. Back-to-back radial bases fed by flower-petal transducers, measured with and without mode filters.

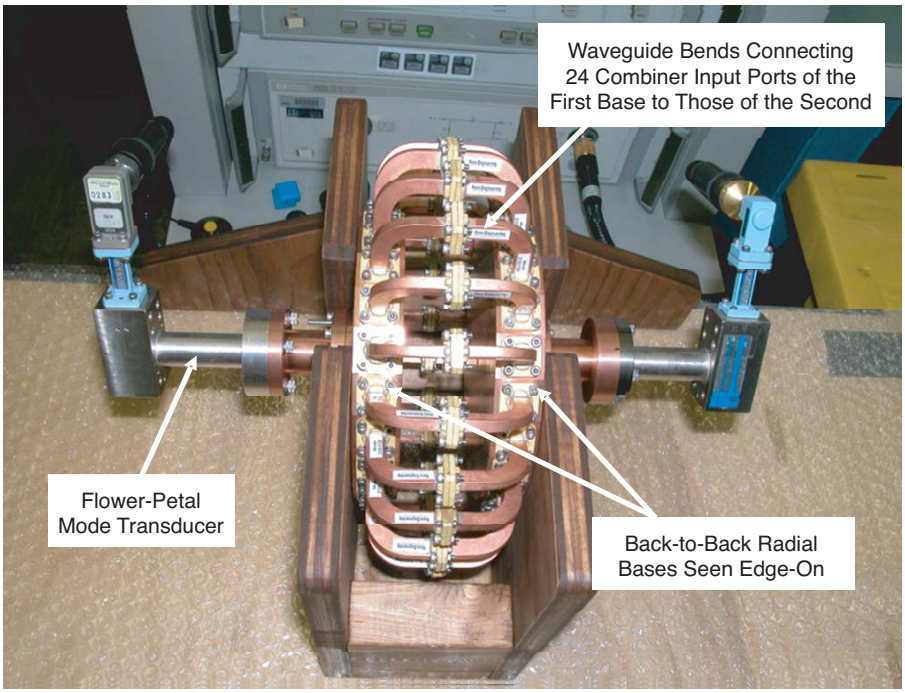

Fig. 4. Photograph of the measurement setup corresponding to Fig. 3, the no-mode-filter case.

radial bases were used in both sets of measurements. Although the Marie transducer operates over the full 31- to 36-GHz band, measurements were limited by the mode filter design to the 33.5- to 35.5-GHz band.

As with the flower-petal transducer, two Marie transducers were measured in a back-to-back configuration with and without the mode filter inserted between the transducers (Fig. 1). Unfortunately, the responses with and without the filter do not appear to be significantly different. Referring back to Fig. 2, it is evident that the mode filter suppressed certain large spurious spikes in the response. However, smaller ($\sim$0.1 dB) spikes were not affected. Furthermore, the filter seemed to introduce additional small ($<$0.1 dB) spikes in the response. Thus, clearly the mode filter, an absorptive helix design, suppresses certain spurious modes and not others. It appears that, in the measured band, back-to-back Marie transducers do not generate significant power in modes for which this specific filter design is effective.

The filtered response in Fig. 5 can be offset by 0.1 dB (the loss of the mode filter) such that the two responses superimpose (Fig. 6). Measured data, thus plotted, seem to indicate that some small spikes generated by the transducers were suppressed by the mode filter.

The transducer response outside the filter operating band contains spikes as large as 0.4 dB (Fig. 7). Measured results suggest that, to suppress these spikes, a new mode filter should be designed that operates not only over the required frequency band of 31 to 36 GHz, but which suppresses spurious modes specifically generated by the Marie transducers.

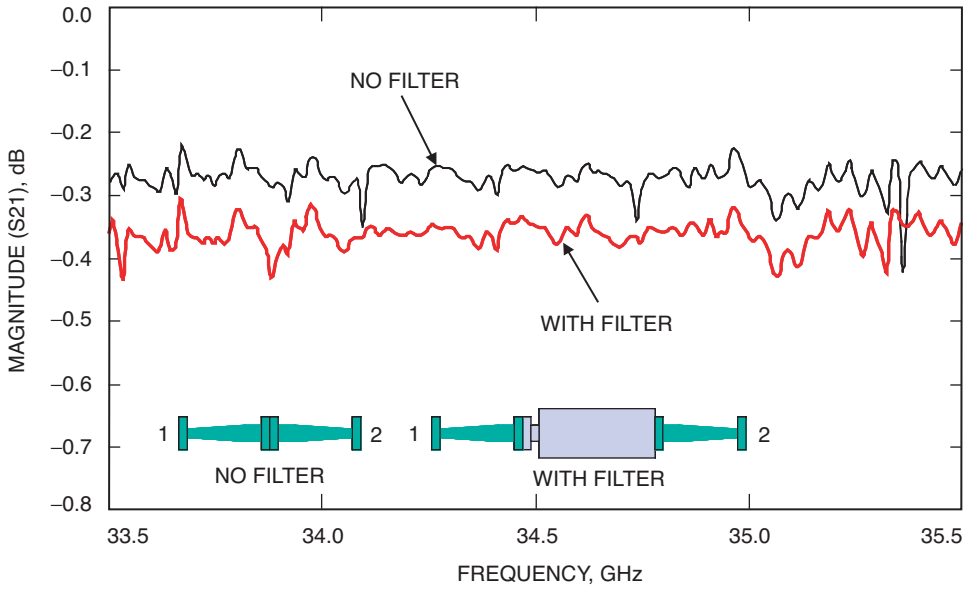

Fig. 5. Back-to-back Marie transducers, measured with and without a mode filter.

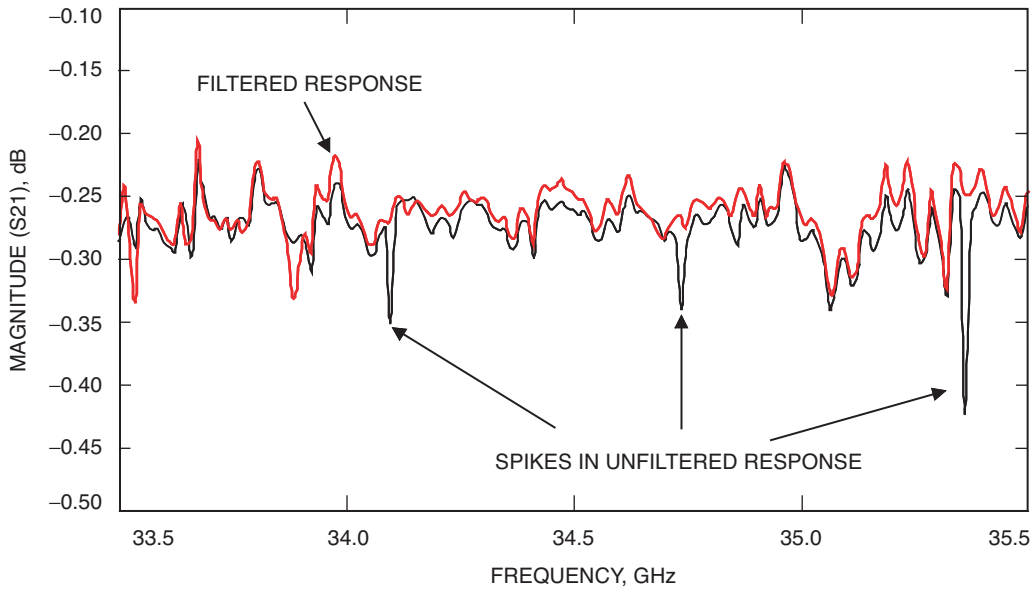

Fig. 6. Data from Fig. 5, with the filtered case offset and the vertical scale expanded. A small amount of power seems to be generated in modes for which the filter is effective.

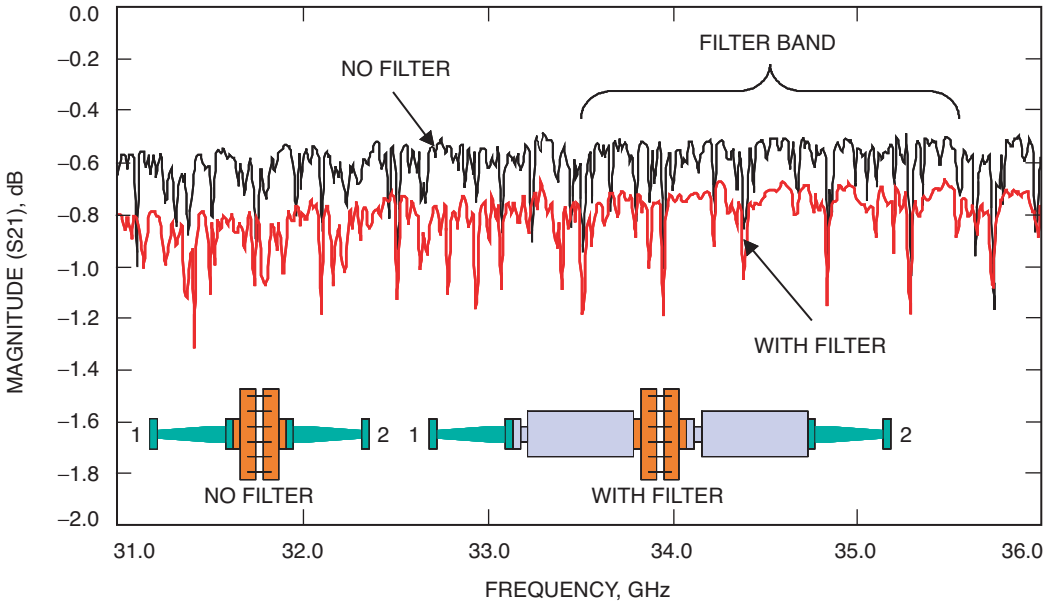

Fig. 7. Back-to-back radial bases fed by Marie transducers.

D. Radial Combiner High-Power Test

The back-to-back configuration of the 24-way radial combiner, fed by the Marie transducer, was tested under high-power excitation at 34.4 GHz (Fig. 8). Measured input and output powers are listed in Table 1.

The prototype radial combiner is purely a waveguide structure with no resistive elements. As such, the power-handling capability of the prototype combiner is expected to be limited by waveguide breakdown only. Due to limitations of the measurement setup, however, the combiner was tested with drive power up to approximately 50 W. Since this level of drive is below the expected limits, anomalous combiner behavior was neither expected nor observed. If a mode filter is used, the power capability of the radial combiner will likely be limited by the power limits of the mode filter.

III. Septum Combiner Activities

A. Septum Combiner High-Power Test

The power-handling capability of the septum combiner is limited by the amount of power that can be dissipated in the septum resistive element without causing damage. Under equal excitation of the combiner input ports (port 1, port 2), very little power is dissipated in the resistive element. The worst-case insertion loss of the combiner is <0.1 dB. Thus, if each input port is excited with 1 W, the total power loss is <46 mW. A fraction of this lost power is dissipated in the resistive element. The remaining power is lost due to port mismatch and finite conductor loss. However, if only one input port is excited while the other is not, approximately half of the drive power is delivered to the output port and the other half is dissipated in the resistive element. Such asymmetry in excitation can arise in a power-combining application due to one or more source failures.

To determine how much power can be safely dissipated in the septum resistive element, a prototype combiner was tested with high-power excitation. The experimental setup is illustrated in Fig. 9. A TWTA amplifier was used as a high-power source to excite only one input port of the combiner, port 2. The match at port 2 was monitored as a function of drive level. The input match is a strong function of the sheet resistance of the resistive element and is, therefore, a good indicator of changes resulting from the power load.

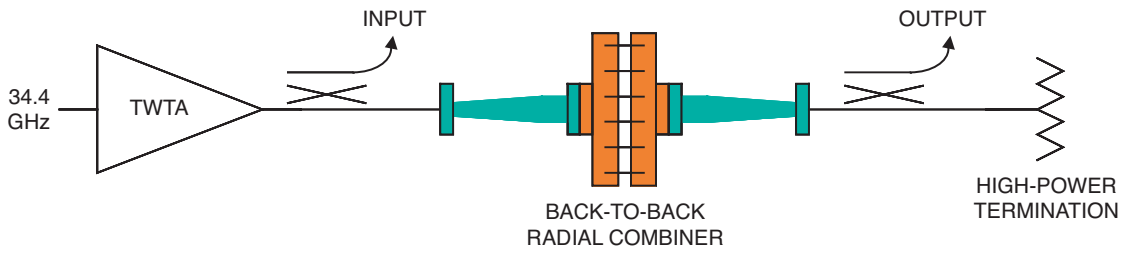

Fig. 8. Measurement setup for radial combiner high-power test.

Table 1. 24-way radial combiner measured input and output powers.

Input power, W	Output power, W
12.15	10.0
18.1	15.0
23.6	20.0
29.4	25.0
35.3	30.0
41.5	35.0
47.7	40.0

Figure 10 illustrates the drive profile and the corresponding response of the prototype combiner as a function of test time. Starting at an initial excitation of 10 W, the drive power was increased in steps until significant degradation in return loss was observed. Each increase in drive power generally was followed by a 5-minute dwell period to allow the system to reach thermal equilibrium. Return loss data points were taken at the end of each dwell period. The initial improvement in return loss, with increasing drive power up to 23 W, could be due to a shift in the resistive element's sheet resistance. However, information from prior test runs suggests that the shift likely is due to instrumentation. Termination of the test below 23 W indicates the shift in combiner performance is not permanent. Moreover, as shown in Fig. 10, the return loss is stable for a 20-W drive, over a 15-minute dwell time. Increasing the drive beyond 23 W, however, results in a gradual degradation of performance. Unlike the performance shift below 23 W, this degradation mode appears to result in a permanent change in performance.

The degradation of return loss, as drive power is increased from 23 W to 29 W, seems to saturate. There are two possible explanations. First, with each unit increase in drive power, as the return loss degrades, a greater fraction of power is reflected and a lesser fraction is dissipated in the resistive element. Second, as return loss degrades, performance of the circuit becomes less sensitive to the value of the resistive element's sheet resistance. Both effects seem to prevent a "runaway" situation and make the mode of combiner degradation gradual and self-limiting. This behavior should contribute to the desired graceful degradation characteristic of the target SSPA.

A more accurate, small-signal measurement of the prototype combiner was taken before and after the high-power test (Fig. 11). The output port match (S11) does not depend on the septum sheet resistance and, thus, remained unchanged, as expected.

The input port match (S22, S33) and isolation (S32), however, degraded to approximately 16 dB. The observed degradation is believed to result from an increase in the tantalum nitride (TaN) film

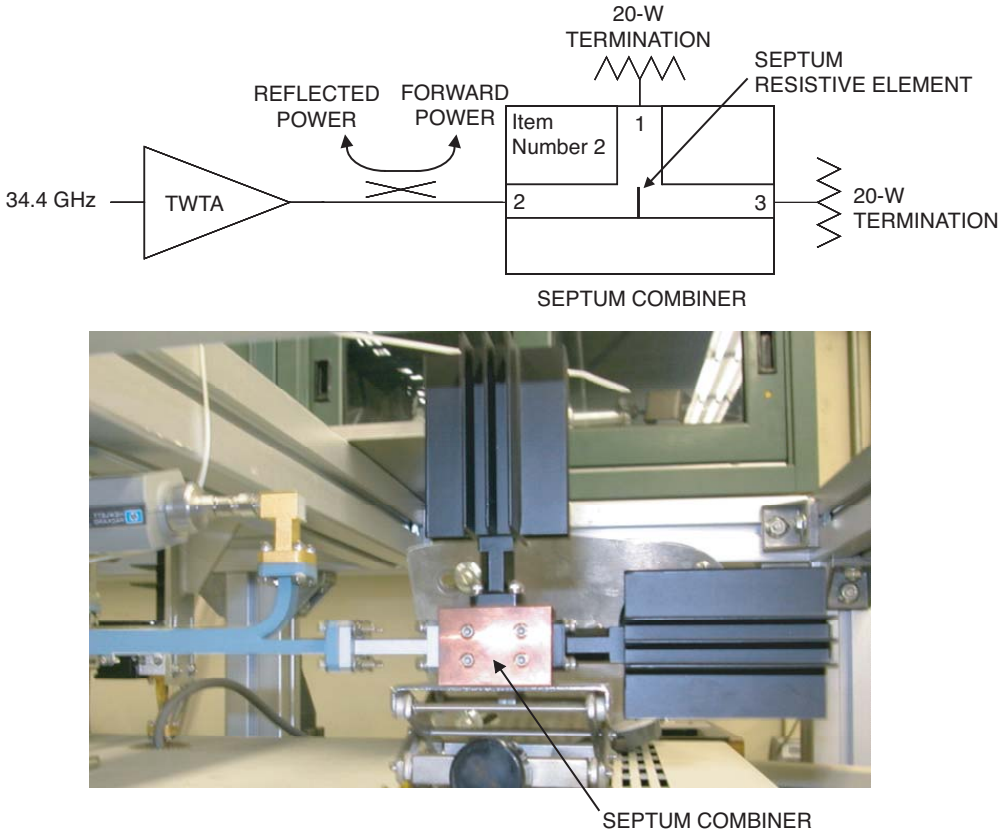

Fig. 9. Septum combiner high-power test setup.

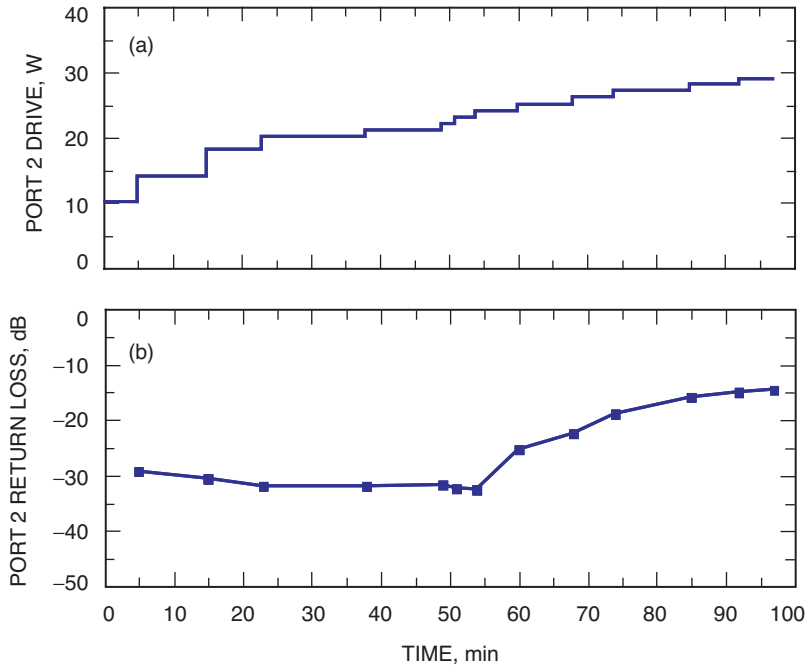

Fig. 10. Septum combiner high-power test results: (a) drive power and (b) combiner response over the duration of the high-power test.

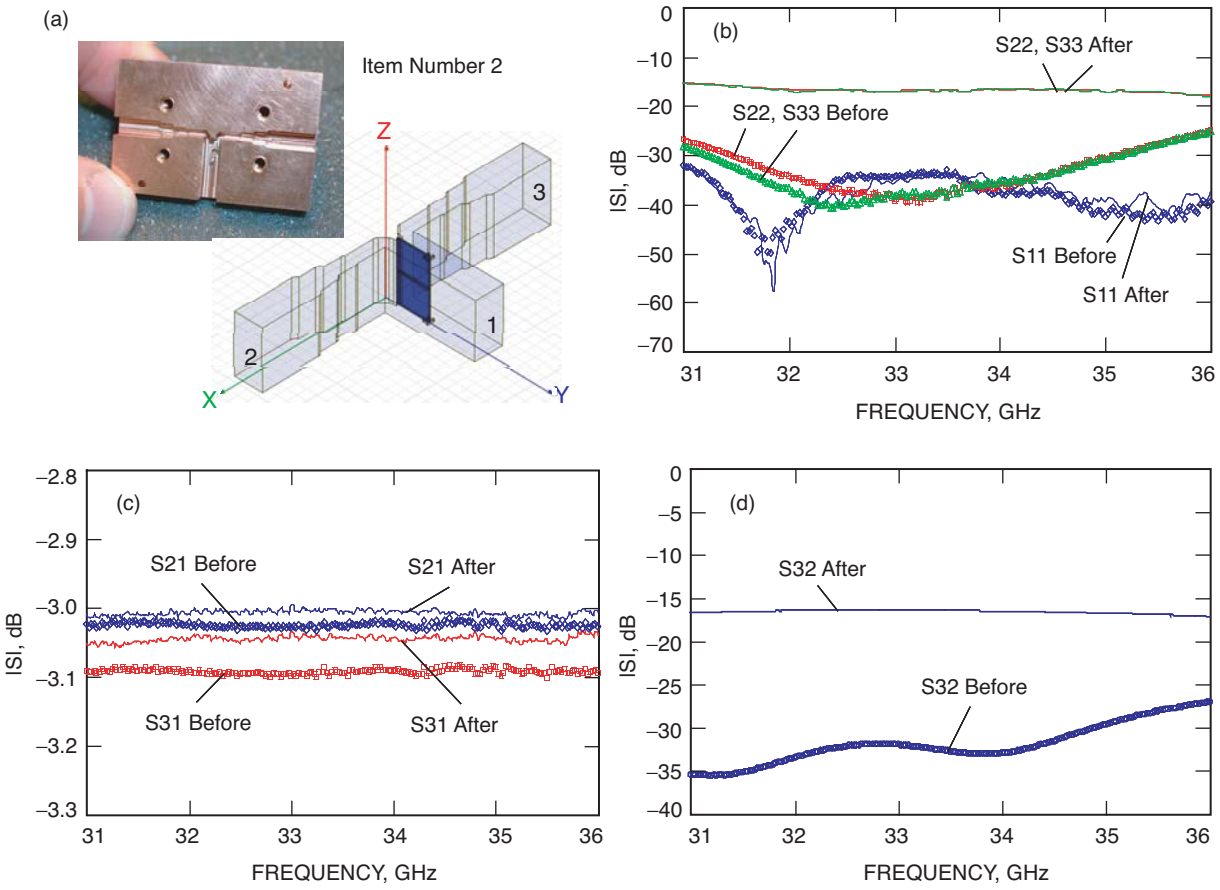

Fig. 11. Comparison of small-signal measurements before and after the high-power test: (a) geometry of the septum combiner being tested, (b) port match, (c) coupling, and (d) isolation.

sheet resistance due to RF heating. An increase in the thickness of the surface oxide layer is a possible mechanism for the change in sheet resistance.

To determine the value of sheet resistance after the high-power test, the value of sheet resistance in the original simulation model was modified until a good match between analysis and measurement was obtained (Fig. 12). The sheet resistance in the model needed to be increased from 128 Ω/sq. (before the high-power test) to 415 Ω/sq. (after the high-power test). This significant, 224 percent increase is consistent with prior observation that the combiner circuit is well-tolerant to variations in the septum sheet resistance. For manufacturing the prototype combiner, the standard ±10 percent tolerance in sheet resistance was found to be sufficient for achieving the design performance. As part of future activities, it should be possible to measure the magnitude and distribution of the modified sheet resistance in the resistive element under test and compare them directly with analysis. The resulting data could be used to optimize the thermal design of the resistive element, if needed.

B. Septum Combiner Architecture Power Constraints

A 2-way septum combiner (adder) can be cascaded in a binary fashion to implement an N-way combiner, where N is constrained to a power of 2. The 8-way combiner case ($N = 8$) is illustrated in Fig. 13. In general, for an N-way combiner, there are $(N - 1)$ identical adders. To ensure the resistive element in no single adder exceeds its power rating, the source powers must be appropriately limited. Based on measurements of the prototype adder, we can estimate the power constraints for a general N-way septum combiner, as discussed below.

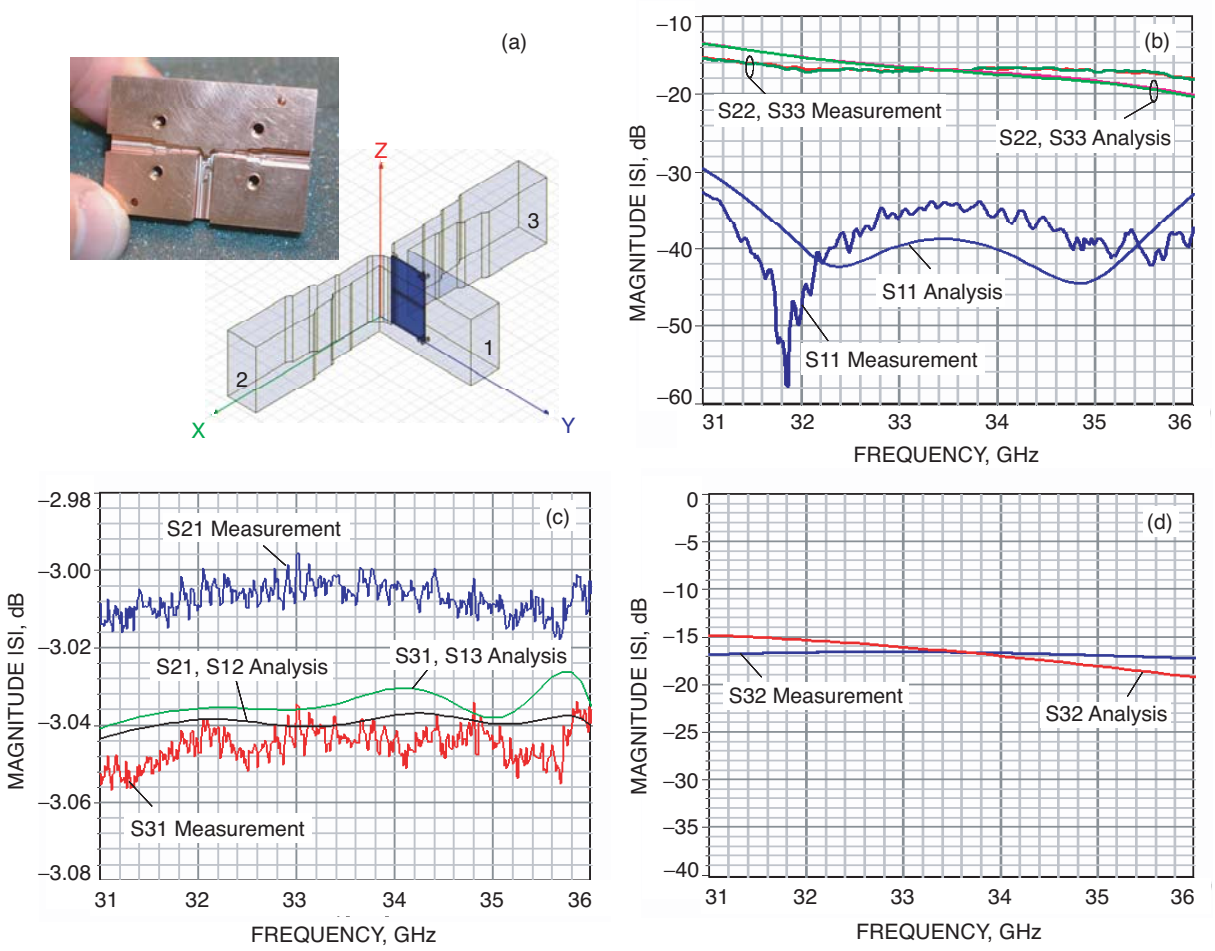

Fig. 12. Comparison of analysis, with the septum sheet resistance modified from the original design and small-signal measurements taken after the high-power test: (a) geometry of the septum combiner being tested, (b) port match, (c) coupling, and (d) isolation.

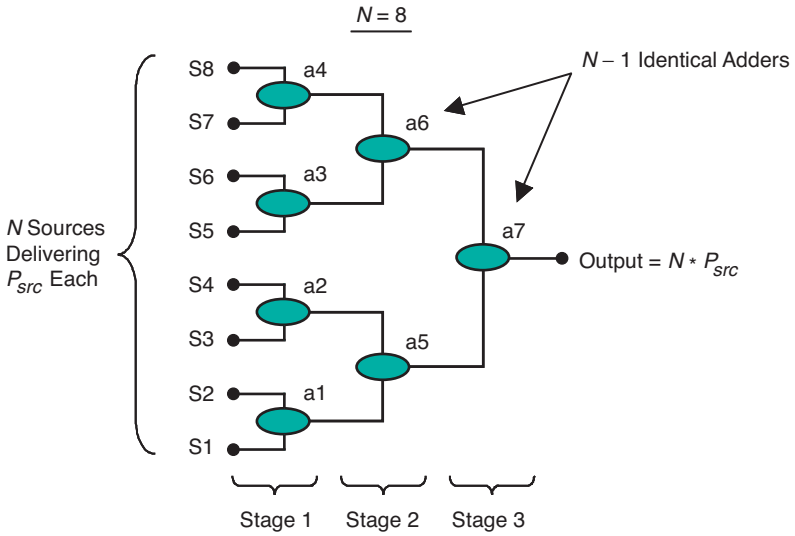

Fig. 13. General layout of an 8-way binary combiner.

Results of the high-power test indicate that a drive imbalance, or differential input ($P_{\text{input1}} - P_{\text{input2}}$), of up to approximately 20 W can be tolerated by an adder (Section III.A). Since nearly half of this power is dissipated in the septum resistive element, the maximum power that can be safely dissipated in the resistive element of a given adder is 10 W.

For symmetric excitation, small-signal measurements indicate the insertion loss of the adder is <0.1 dB (Fig. 12). A fraction of this lost power is dissipated in the resistive element. The remainder is lost due to port mismatch and finite conductor loss. Making the conservative assumption that all lost power is dissipated in the resistive element, we note that, for symmetric excitation, up to 5 percent of the power at each input port of a given adder is dissipated in its resistive element. Thus, in theory, a given adder can combine two sources producing 200 W (=10 W/0.05) each, provided the source powers are equal at all time. The maximum combined output possible in this theoretical case is, therefore, 400 W.

To ensure the root adder in the final stage of an N-way binary combiner does not exceed this limit, the source power must be limited to the following. Constraint 1:

$$P_{src} \leq \frac{400}{N \cdot (L_s)^{n_s}} \text{ watts} \tag{1}$$

where

$P_{src} =$ source power at each input

$N =$ number of sources combined

$n_s =$ number of stages $= \log_2(N)$

$L_s =$ average insertion loss per stage

Constraint 1 ensures that the power limit of the root adder will not be exceeded under normal, symmetric operation (i.e., with no source failures). Adders at earlier stages dissipate successively lower power.

Asymmetric drive resulting from source failures, however, potentially can damage adders at any stage of the binary tree. The specific adder expected to be damaged depends on the source power, the number of source failures, and the failure distribution. If the combiner is required to withstand these failures without damage, the source power must be further limited. We note that a given adder experiences maximum drive asymmetry when all sources feeding one input branch fail while all sources feeding the other branch produce full power. The probability of this failure distribution decreases with an increasing number of failures under consideration. However, to be conservative, we will assume this worst-case failure distribution for the following analysis.

Constraint 1 allows P_{src} to exceed 20 W (i.e., for $N \leq 16$). However, with $P_{src} > 20$ W, a first-stage adder can be damaged if one of its two sources fails. Thus, to tolerate at most one failure, P_{src} cannot exceed 20 W. For two source failures, the maximum drive asymmetry of $2P_{src}$ is experienced by a second-stage adder. Thus, to tolerate at most two failures, P_{src} cannot exceed 10 W. The case of three failures does not increase the magnitude of asymmetry in the system as compared with two failures. In general, for an N-way combiner, the maximum asymmetry is experienced by the root adder when $N/2$ sources on one half of the binary tree fail. Additional failures in the other half of the tree actually decrease asymmetry. Thus, for guaranteed immunity against an arbitrary number of failures, the source power cannot exceed $20/(N/2) = 40/N$ W.

In general, to ensure the resistive element in no single adder exceeds its power rating, the following constraint must be observed in addition to constraint 1. Constraint 2:

$$P_{src} \leq \frac{20}{n_f \cdot (L_s)^{n_{sf}}} \text{ watts}, \quad n_f = 2, 4, 8 \cdots \frac{N}{2} \tag{2}$$

$$P_{src} \leq \frac{40}{N \cdot (L_s)^{n_{sf}}} \text{ watts}, \quad \frac{N}{2} < n_f \leq N \tag{3}$$

where

$P_{src} =$ source power at each input

$N =$ number of sources combined

$n_f =$ maximum number of source failures allowed

$n_{sf} = \log_2(n_f)$, the number of stages between the source and power limiting adder

$L_s =$ average insertion loss per stage

The maximum source and output power for various N and n_f are tabulated in Table 2. For a 140-W SSPA, a 16-way combiner ($N = 16$) could be used to power combine 10-W sources. According to Table 2, up to three such sources can fail without overloading any resistive element in the combiner. Alternatively, a 32-way combiner ($N = 32$) can be used to power combine 5-W sources. For this configuration, up to seven sources can fail without overloading any resistive element.

Assuming the source failures are independent, the probability of n_f failures is equal to the probability of a single failure raised to the power n_f. The worst-case scenario of n_f failures, therefore, quickly

Table 2. Maximum source power and maximum combined output power for guaranteed safe operation, as a function of number of sources combined (*N*) and the maximum number of source failures allowed (n_f).

N	n_f	P_{src} max, W	P_{out} max, W
2	1	20.0	39
4	1	20.0	76
	2–3	10.3	39
8	1	20.0	147
	2–3	10.3	76
16	1	20.0	287
	2–3	10.3	147
32	1	14.4	400
	2–3	10.3	287
	4–7	5.3	147

Note: Calculation assumes $L_s = 0.12$ dB average loss per combiner stage; P_{out} max is the maximum SSPA output with no source failure.

becomes highly improbable as n_f increases. It seems unlikely that a real system will be designed with an expectation of greater than at most three failures. Therefore, depending on the source power available, either a 16-way or a 32-way combiner could be used to implement the target SSPA and guarantee safe operation in the event of multiple source failures.

C. Improved Design for Manufacturability

The prototype septum combiner fabricated during the initial phase of this study employed split-block fabrication in which the top and bottom halves of the waveguide blocks were fabricated separately. The resistive septum in this original design also was implemented in two halves. A pair of alumina substrates with the TaN resistive sheet in between (forming the bottom half of the septum) was integrated with the bottom waveguide block [Fig. 14(a)]. An identical pair of substrates forming the top half of the septum was integrated with the top waveguide block. This approach allows the septum substrates to be integrated with waveguide blocks before the waveguide blocks are mated [Fig. 14(b)].

A benefit of the original design is that disruptions in the waveguide wall (e.g., due to slots) are minimized. This simplifies the electrical design and increases the likelihood that the fabricated part will more closely reproduce the designed performance. A drawback, however, is that great care is needed to integrate the septum with the waveguide. Not only must two sets of substrates be integrated with the waveguide blocks, the substrates must be fixed to the metal structure with careful application of epoxy or silicone room temperature vulcanising (RTV). This greatly increases the assembly time.

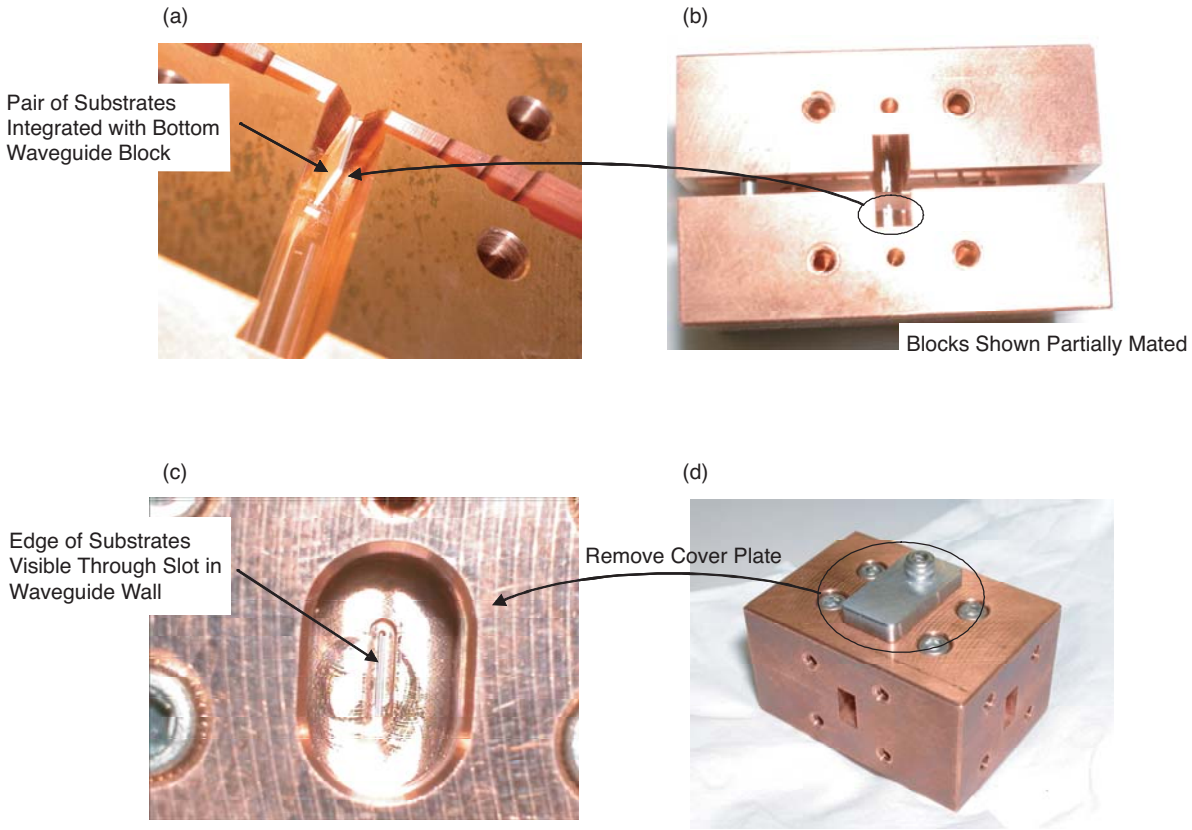

Fig. 14. The prototype septum combiner. (a) and (b): the original, split-card method of integrating the septum. Two substrate pairs (one pair forming the upper and one pair forming the lower half of the septum) are separately integrated with each waveguide block *before* the blocks are mated. (c) and (d): the new, improved, slot-insertion method of integrating the septum. A single substrate pair (forming the full septum) is inserted through a slot on the waveguide wall *after* the waveguide blocks are mated.

A new design was implemented that addresses the manufacturing issues. In the new design, the waveguide structure is manufactured as in the original design, i.e., as split-blocks. However, the blocks are mated first without the septum substrates. A single pair of substrates (forming the full septum) then is inserted through a slot in the narrow wall of the waveguide structure [Figs. 14(c) and 14(d)]. The structure is designed such that the substrates are held captive by the waveguide metal. The use of epoxy within the waveguide therefore is not required. A cover plate, illustrated in Fig. 14(d), is used to cap the slot. Although the structure does not require that epoxy be used, it may be prudent to do so for increased thermal conductivity and to eliminate small performance variations that may result from potential card movements. The epoxy, however, need not be applied with the care required in the original design. In the new design, since the epoxy can be placed in the slots, outside the waveguide volume, the epoxy does not interact effectively with electromagnetic fields.

The new design reduces the individual substrate count from 4 to 2 per adder and decreases the assembly time from over 2 hours to approximately 15 minutes per adder.

Tables 3 and 4 list the small-signal RF performances of the original and the new designs, respectively. The match, coupling, and isolation performances of the two designs are comparable. However, the unit-to-unit variability in the new design is greater as compared with the original design.

Table 3. Measured RF performance of the original, split-block assembled septum design (worst-case values over the 31- to 36-GHz band).

Item number	Match, dB			Coupling, dB		Isolation, dB	Amplitude balance, dB	Phase balance, deg
	S11	S22	S33	S12	S13	S23	|S12 − S13|	|S12 − S13|
1	−31	−25	−25	−3.055	−3.060	−27	0.005	0.75
2	−31	−25	−25	−3.030	−3.095	−27	0.065	0.2
3	−31	−25	−25	−3.045	−3.060	−27	0.015	0.49
4	−31	−25	−25	−3.047	−3.044	−27	0.003	0.27
Average	−31	−25	−25	−3.044	−3.065	−27	0.022	0.43

Table 4. Measured RF performance of the new, slot-inserted septum design (worst-case values over the 31- to 36-GHz band).

Item number	Match, dB			Coupling, dB		Isolation, dB	Amplitude balance, dB	Phase balance, deg
	S11	S22	S33	S12	S13	S23	|S12 − S13|	|S12 − S13|
1	−31	−26	−26	−3.100	−2.990	−29	0.110	1.57
2	−30	−22	−22	−3.020	−3.070	−22	0.050	2.13
3	−30	−25	−25	−3.100	−3.080	−27	0.020	3.23
4	−31	−23	−24	−3.040	−3.090	−24	0.050	2.43
Average	−31	−24	−24	−3.065	−3.058	−26	0.057	2.34

The increased variability in the new design is likely due to two causes. First, for the measured set of prototype combiners, the septum substrates were not fixed with epoxy as recommended above. Second, the width of one of the two substrates that comprise the septum was out of specification by 0.127 mm (the specified tolerance is ±0.025 mm). The resulting asymmetry in the septum structure is believed to have contributed to the degraded amplitude and phase balance. If substrates are fabricated to proper dimensions and they are fixed in place with epoxy, the variability in the new design is expected to improve.

IV. Conclusions

Measurements of the prototype radial combiner demonstrated that a mode filter can greatly reduce spurious mode effects. To realize this improvement, however, the filter must be properly matched to the frequency response and mode content of the transducer. In back-to-back radial combiner measurements, a commercial mode filter, used in conjunction with its corresponding mode transducer, reduced spikes in the passband from up to 1.75-dB magnitude to less than 0.2 dB (Fig. 3). The same mode filter, however, did not significantly reduce spurious spikes when used in conjunction with the broadband Marie transducer. This particular commercial mode filter does not appear to operate over the full bandwidth of the Marie transducer, and the specific set of modes that is suppressed by this filter likely is not the same as the set of modes generated by the Marie transducer. To reduce spurious modes in broadband SSPA applications, therefore, a custom mode filter, matched to the frequency and mode set of the Marie transducer, will need to be designed.

The high-power test of the radial combiner was limited by the available source power. The 24-way prototype combiner was tested in a back-to-back configuration with drive power up to approximately 50 W. No anomalous behavior was observed. In the future, the combiner should be tested (including the mode filter, if one is used) with drive power greater than 140 W to ensure the combiner can meet requirements of the target application. The waveguide structures of the combiner (the mode transducer and radial base) are expected to be breakdown-limited. Thus, the power limit of the mode filter, if one is used, likely will be the limiting factor.

High-power tests of the prototype septum combiner indicate that up to 10 W can be dissipated by the resistive element at each adder in an N-way binary combiner. Under normal, symmetric excitation, <5 percent of the source power is dissipated by the resistive element. Thus, in theory, an SSPA producing up to 400 W can be implemented. To allow for the possibility of source failures, however, this power must be significantly reduced. Calculations show that for a 140-W SSPA, based on a 16-way septum combiner, up to three sources can fail with a guarantee that the combiner will not be damaged. If a 32-way combiner is used, up to seven can fail with a guarantee that the combiner will not be damaged. These restrictions assume a specific failure distribution that maximizes the power imbalance at a given adder. Thus, in practice, it is probable that more failures can be tolerated by the combiner, without damage, than these limits permit. Furthermore, exceeding the power limit was demonstrated to cause a gradual degradation of the combiner performance. These results suggest that the septum combiner is well-suited to space applications where graceful degradation of the SSPA is advantageous. The effect of source failures on system performance should be analyzed in greater detail and verified in the future.

Finally, a modified septum combiner design was verified. The new design allows the septum combiner resistive element to be integrated more easily. The design modification decreased assembly time from over 2 hours to approximately 15 minutes per adder. This modification increases the ease with which a high-order (large N) combiner can be implemented.

Acknowledgments

The authors would like to acknowledge the following individuals for making significant contributions to the work documented in this article: Daniel J. Hoppe, JPL; Richard D. Rebele, JPL; and Dan Kelley, Honeywell Technology Solutions, Inc.

References

[1] P. Khan, L. Epp, and A. Silva, "A Ka-Band Wideband-Gap Solid-State Power Amplifier: Architecture Identification," *The Interplanetary Network Progress Report*, vol. 42-162, Jet Propulsion Laboratory, Pasadena, California, pp. 1–16, August 15, 2005. http://ipnpr/progress_report/42-162/162E.pdf

[2] P. Khan, L. Epp, and A. Silva, "Ka-Band Wideband-Gap Solid-State Power Amplifier: General Architecture Considerations," *The Interplanetary Network Progress Report*, vol. 42-162, Jet Propulsion Laboratory, Pasadena, California, pp. 1–19, August 15, 2005.
http://ipnpr/progress_report/42-162/162F.pdf

[3] P. Khan, L. Epp, and A. Silva, "A Ka-Band Wide-Bandgap Solid-State Power Amplifier: Architecture Performance Estimates," *The Interplanetary Network Progress Report*, vol. 42-163, Jet Propulsion Laboratory, Pasadena, California, pp. 1–17, November 15, 2005.
http://ipnpr/progress_report/42-163/163A.pdf

[4] L. Epp, P. Khan, and A. Silva, "A Ka-Band Wide-Bandgap Solid-State Power Amplifier: Hardware Validation," *The Interplanetary Network Progress Report*, vol. 42-163, Jet Propulsion Laboratory, Pasadena, California, pp. 1–22, November 15, 2005. http://ipnpr/progress_report/42-163/163B.pdf

[5] *340 Series Mode Filter Data Sheet*, Millimeter Products, Inc. (MPI). http://www.milpi.com/340main.html. MPI is now part of QuinStar Technology, Inc., Torrance, California.

[6] *330 Series TE_{01} Mode Transition Data Sheet*, Millimeter Products, Inc. (MPI). http://www.milpi.com/330main.html. MPI is now part of QuinStar Technology, Inc., Torrance, California.

[7] H. A. Hoag, S. G. Tantawi, R. Callin, H. Deruyter, Z. D. Farkas, K. Ko, N. Kroll, R. L. Lavine, A. Menegat, and A. E. Vlieks, "Flower-Petal Mode Converter for NLC," *Proceedings of the 1993 Particle Accelerator Conference*, vol. 2, pp. 1121–1123, May 17-20, 1993.